C. R. Chimie 17 (2014) 964–970

Contents lists available at ScienceDirect

Comptes Rendus Chimie

www.sciencedirect.com

Full paper/Mémoire

Synthesis of ZnS nanoparticles from pyridine adducts of zinc(II) dithiocarbamates

Narayanaswamy Srinivasan, Subbiah Thirumaran *

Department of Chemistry, Annamalai University, Annamalinagar 608 002, Tamilnadu, India

ARTICLE INFO

Article history:
Received 7 May 2013
Accepted after revision 17 October 2013
Available online 26 June 2014

Keywords:
Zinc dithiocarbamate
Precursors
ZnS nanoparticles
Optical properties

ABSTRACT

$Zn(thqdtc)_2$, $Zn(thqdtc)_2(py)$ and $Zn(thiqdtc)_2(py)$ (where thqdtc = 1,2,3,4-tetrahydroquinolinecarbodithioate, thiqdtc = 1,2,3,4-tetrahydroisoquinolinecarbodithioate and py = pyridine) have been used as single source precursors for the synthesis of ZnS nanoparticles. The formation of ZnS nanoparticles was achieved by thermal decomposition of the complex under heating in presence of triethylenetetraamine. Transmission electron microscopy, energy dispersive X-ray analysis (EDAX) and powder X-ray diffraction studies were carried out to study the structure and morphology of the nanoparticles. The optical properties of the ZnS nanoparticles were studied by UV–visible and fluorescence emission spectral studies. UV–visible absorption spectral studies indicate a blue shift in the absorption maxima due to the quantum size effect. A single crystal X-ray analysis was carried out for a precursor $[Zn(thqdtc)_2]$.

1. Introduction

Recently, two-dimensional nanostructured materials, such as nanotubes, nanorods and nanowires, have attracted considerable interest because of their unique physical properties and potential applications in optics, magnetics and electronics [1–3]. Semiconductor nanoparticles have prospective applications in many technological areas, including photo- and electroluminescent devices, light-emitting diodes, and photovoltaic devices [4–6]. Especially, due to a wide-band gap (bulk band gap = 3.6 eV), ZnS nanoparticles are good emitters of light in blue and ultraviolet ranges, so they have found many applications, for instance as phospors, solar cells, and infrared windows, as the properties of nanoparticles are highly dependent on their structure, size and size distribution, and morphology. Studies on the nanoparticle synthesis, growth, and microstructural evolvement play a critical role in controlling the size-dependent properties [7–9]. Recently, various methods have been developed to synthesize different structures of semiconductor nanoparticles, including sol–gel templates, thermolysis of metal complexes, solvothermal, micelle–template interface, reduction route, ion beam synthesis, ultrasonic irradiation in an aqueous solution, etc. [10–15]. Several groups have reported the synthesis of metal sulfide nanoparticles from the thermal decomposition of single source precursors using a conventional heating process [16–18]. The use of single source precursors containing both metal and chalcogenide source (metal–ligand complexes) has been extensively studied as an effective route to the synthesis of nanoparticles. The properties of the ligand in metal complexes used as precursors could be used in the modification of the size and shape of the nanoparticles. For example, a variation of the alkyl groups on the dithiocarbamate ligand was found to give particles with non-spherical morphologies [19].

In this work, we have used three different precursors, $Zn(thqdtc)_2$, $Zn(thqdtc)_2(py)$, and $Zn(thiqdtc)_2(py)$ complexes as single source precursors for the synthesis of ZnS nanoparticles. This is the first report of the use of pyridine adducts of zinc-heterocyclicdithiocarbamates for the synthesis of ZnS nanoparticles. The single crystal X-ray structure of $Zn(thqdtc)_2$ is also reported.

* Corresponding author.
E-mail address: sthirumaran@yahoo.com (S. Thirumaran).

1631-0748/$ – see front matter
http://dx.doi.org/10.1016/j.crci.2013.10.009

2. Experimental

2.1. General

1,2,3,4-Tetrahydroquinoline (Alfa Aesar), 1,2,3,4-tetrahydroisoquinoline (Sigma–Aldrich), carbon disulfide (Merck), pyridine (Merck), and solvents (sd fine) were commercially available high-grade materials and were used as received. The wide-angle X-ray diffraction (XRD) was recorded using a Philips X'pert Pro MPD Diffractometer. The diffraction pattern over the 2θ range of 10–80° was recorded at a scan rate of 5 s/step. TEM images were recorded using a Philips CM200 (operating voltages: 20–200 kV, resolution: 2.4 Å). Energy dispersive X-ray spectroscopy (EDAX) measurements were performed using a JEOL model JED-2300 instrument. A Shimadzu UV-1650 PC double beam UV–Visible spectrophotometer was used for recording the electronic spectra. The spectra were recorded in chloroform and the pure solvent was used as the reference. Fluorescence measurements were made using a Jasco FP-550 spectrofluorimeter.

2.2. X-Ray crystallography

Details of the crystal data, data collection and refinement parameters for the $Zn(thqdtc)_2$ complex are summarized in Table 1. Suitable crystals were obtained through slow evaporation of a dichloromethane solution of $Zn(thqdtc)_2$. The intensity data were collected at ambient temperature [293(2) K] on a Bruker AXS kappa apex2 CCD diffractometer using the graphite monochromated Mo Kα radiation (λ = 0.71073 Å). The structure was solved by SIR-92 [20] and refined by full-matrix least-square method with SHELXL-97 [21]. All non-hydrogen atoms were refined anisotropically and hydrogen atoms were refined isotropically. Selected bond distances and angles are given in Table 2.

Table 1
Crystal data, data collection and refinement parameters for $[Zn(thqdtc)_2]$.

Empirical formula	$C_{20}H_{20}N_2S_4Zn$
FW	481.99
Crystal dimensions (mm)	0.30 × 0.20 × 0.16
Crystal system	Triclinic
Space group	$P\bar{1}$
a/Å	7.636(5)
b/Å	7.637(4)
c/Å	17.681(3)
α/°	85.863(4)
β/°	83.604(3)
γ/°	86.855(7)
U/Å^3	1020.8(9)
Z	2
DC/g cm^{-3}	1.568
μ/cm^{-1}	1.620
F(0 0 0)	4 9 6
λ/Å	Mo K_α (0.71073)
θ range/°	1.16 – 25.00
Index ranges	$-9 \le h \le 9$, $-9 \le k \le 9$, $-21 \le l \le 20$
Reflections collected	3584
Observed reflections $F_o > 4'O(F_o)$	3253
Weighting scheme	Calc. $W = 1/(\sigma^2(F_o^2) + (10.1061p)^2 + 7.548p)$ where $p = (F_o^2 + 2F_c^2)/3$
Number of parameters refined	245
Final R, R_w(obs, data)	0.0257, 0.0302
GOOF	1.122

Table 2
Bond distances (Å) and angles (°) for $[Zn(thqdtc)_2]$.

Bond distances (Å)		Bond angles (°)	
S1–Zn1	2.3024(9)	S1–Zn1–S3	128.84(3)
S2–Zn1	2.3530(12)	S1–Zn1–S4	127.54(3)
S3–Zn1	2.3316(11)	S3–Zn1–S4	77.87(2)
S4–Zn1	2.3450(17)	S1–Zn1–S2	78.37(3)
C19–N2	1.436(3)	S3–Zn1–S2	123.76(3)
C20–N2	1.327(3)	S4–Zn1–S2	128.15(3)
C20–S3	1.720(2)	C10–S2–Zn1	81.48(8)
C20–S4	1.720(2)	C20–S3–Zn1	82.46(8)

2.3. Preparation of $Zn(thqdtc)_2$ and its pyridine adduct

2.3.1. Preparation of $Zn(thqdtc)_2$

An aqueous solution of $ZnSO_4 \cdot 7\ H_2O$ (10 mmol, 2.9 g) was added dropwise to an aqueous solution of $Na(thqdtc) \cdot 2H_2O$ at the temperature of ice cold water. The reaction mixture was stirred for 1 h and the precipitate was filtered. The product was washed several times with cold water and then dried [22]. The yield was 72%.

2.3.2. Preparation of $Zn(thqdtc)_2(py)$

$Zn(thqdtc)_2$ (1 mmol, 0.48 g) was dissolved in 50 mL of warm pyridine. The yellow solution obtained was filtered and kept for evaporation. After a few days, both powder and single crystals suitable for X-ray structural analysis were obtained [23] (Scheme 1). The yield was 65%.

2.4. Preparation of $Zn(thiqdtc)_2$ and its pyridine adduct

2.4.1. Preparation of $Zn(thiqdtc)_2$

An aqueous solution of $ZnSO_4 \cdot 7\ H_2O$ (10 mmol, 2.9 g) was added dropwise to an aqueous solution of $Na(thiqdtc) \cdot 2\ H_2O$ (20 mmol, 5.34 g) at the temperature of ice cold water. The reaction mixture was stirred for 1 h and the precipitate was filtered. The product was washed several times with cold water and then dried [22]. The yield was 68%.

2.4.2. Preparation of $Zn(thiqdtc)_2(py)$

$Zn(thiqdtc)_2$ (1 mmol, 0.48 g) was dissolved in 50 mL of warm pyridine. The yellow solution obtained was filtered and kept for evaporation. After a few days, both powder and single crystals suitable for X-ray structural analysis were obtained [23] (Scheme 2). The yield was 71%.

2.5. Preparation of ZnS nanoparticles

2.5.1. Preparation of ZnS1

An amount of 0.5 g of $Zn(thqdtc)_2$ was dissolved in 15 mL of triethylenetetramine in a flask and then

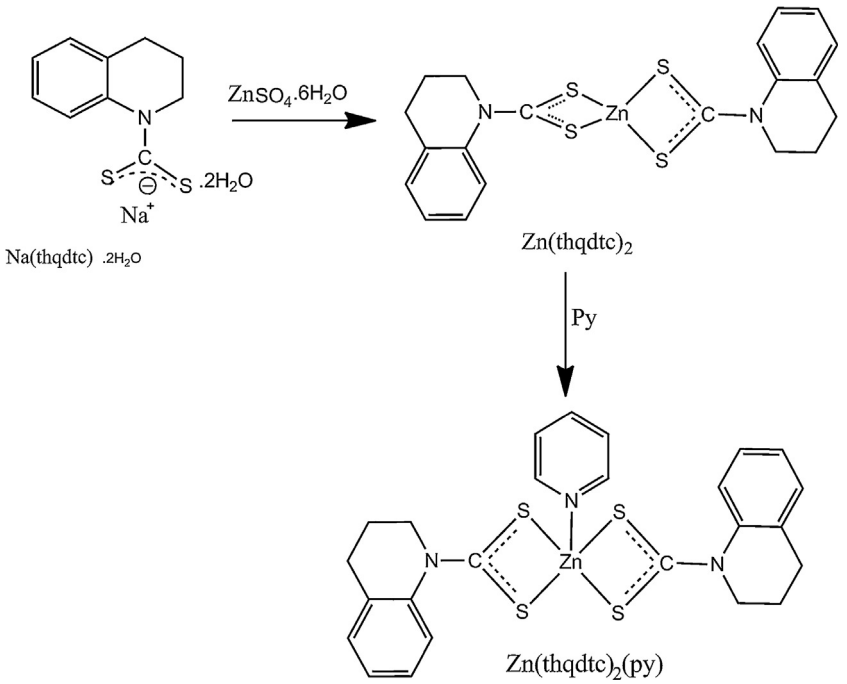

Scheme 1. Preparation of $Zn(thqdtc)_2$ and $Zn(thqdtc)_2(py)$.

heated to reflux (267 °C) and maintained at this temperature for 2 min. The white precipitate obtained was filtered off and washed with ethanol. The yield was 0.075 g.

2.5.2. Preparation of ZnS2

A method similar to that described for the synthesis of ZnS**1** was adopted; however, 0.5 g of $Zn(thqdtc)_2(py)$ was used instead of $Zn(thqdtc)_2$. A white precipitate of nanoparticles was obtained. The yield was 0.066 g.

2.5.3. Preparation of ZnS3

A method similar to that described for the synthesis of ZnS**1** was adopted; however, 0.5 g of $Zn(thiqdtc)_2(py)$ was used instead of $Zn(thqdtc)_2$. A white precipitate of nanoparticles was obtained. The yield was 0.070 g.

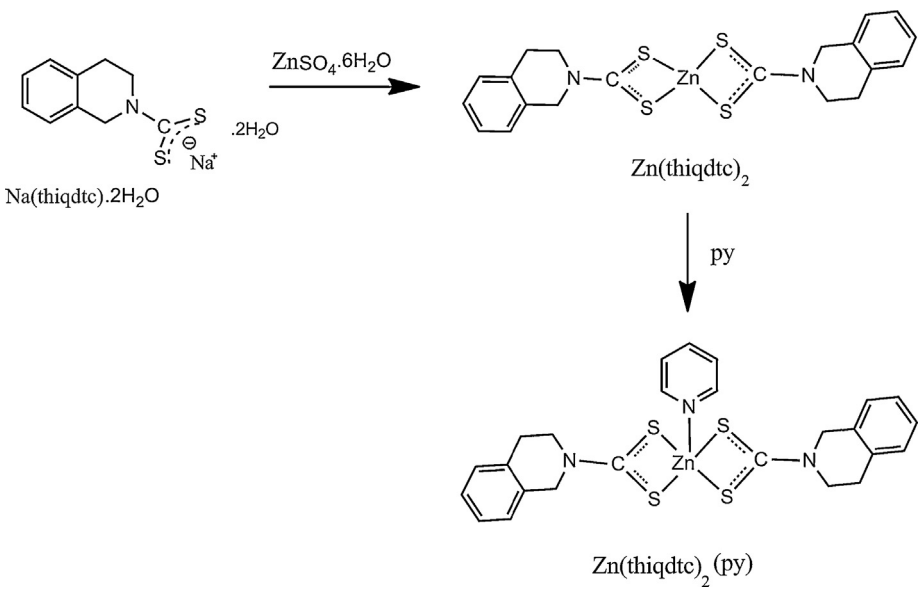

Scheme 2. Preparation of $Zn(thiqdtc)_2$ and $Zn(thiqdtc)_2(py)$.

3. Results and discussion

3.1. Characterization of zinc sulfide nanoparticles

3.1.1. Powder X-ray diffraction analysis

To study the crystalline structures of the products, XRD measurements were carried out at room temperature. The ZnS nanoparticles synthesized from $Zn(thqdtc)_2$, $Zn(thqdtc)_2(py)$, and $Zn(thiqdtc)_2(py)$ are represented as ZnS**1,** ZnS**2** and ZnS**3**, respectively. Fig. 1 shows the XRD patterns of the ZnS**1,** ZnS**2** and ZnS**3**, in which the diffraction peaks marked by "*", "+" and "#" match well cubic (JCPDS Card No: 05-0566), hexagonal (JCPDS Card No: 12-0688) and rhombohedral ZnS (JCPDS Card No: 83-1700) phases, respectively. By examining the whole X-ray diffraction patterns, it is concluded that these nanoparticles contain a mixture of cubic, hexagonal, and rhombohedral phases.

Triethylenetetramine is a strong chelating neutral ligand. It forms a hexacoordinated intermediate complex

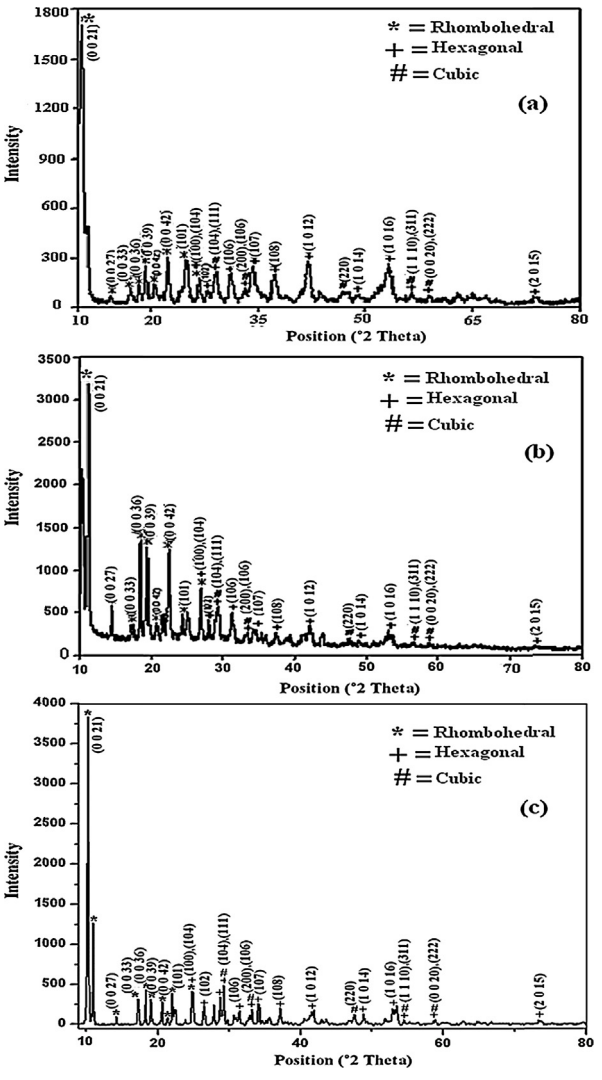

Fig. 1. XRD patterns of (a) ZnS**1,** (b) ZnS**2**, and (c) ZnS**3**.

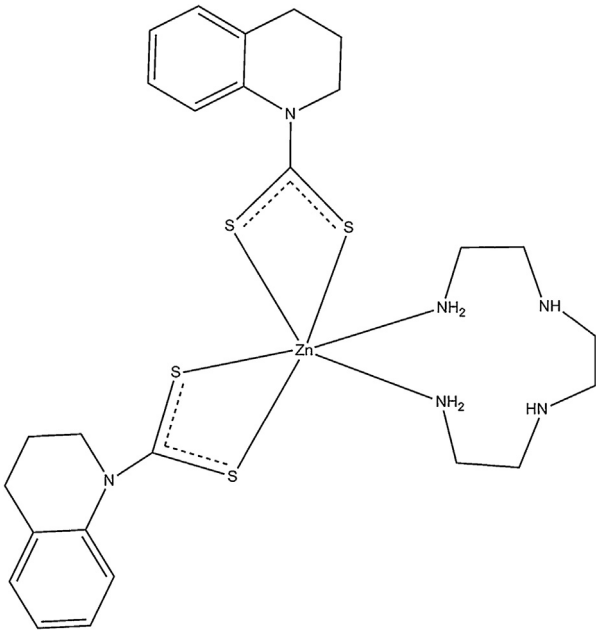

Fig. 2. Proposed structure for the intermediate complex.

(Fig. 2) with $Zn(thqdtc)_2$. $Zn(thqdtc)_2(py)$ also forms the same intermediate complex (Fig. 2) and gives free pyridine. The intermediate complex formed from $Zn(thqdtc)_2$ and $Zn(thqdtc)_2(py)$ depletes at higher temperature (267 °C) when the nucleation process starts. In the powder X-ray diffraction pattern, sharp (0 0 36), (0 0 39), (0 0 42) (rhombohedral phase) peaks are observed for ZnS**2** compared to those in ZnS**1**, indicating that free pyridine in the intermediate stage may bind to the planes of hexagonal and cubic phases of the nucleus, leaving the (0 0 36), (0 0 39), (0 0 42) (rhombohedral phase) more exposed for ZnS deposition in ZnS**2.**

3.1.2. Energy dispersive X-ray (EDAX) analysis

Examination by EDAX of ZnS**1**, ZnS**2** and ZnS**3** confirms the formation of ZnS. The EDAX spectra of ZnS**1**, ZnS**2** and ZnS**3** are shown in Fig. 3. EDAX reveals the presence of zinc and sulfur in all cases. C, N and O signals are also observed in the energy dispersive X-ray spectra of all the as-synthesized zinc sulfides. The presence of C and N peaks in the spectrum evidences the presence of triethylenetetramine in the product. A relatively weak oxygen peak in both spectra probably originates from an unavoidable surface adsorption of oxygen to the zinc sulfide particles when exposed to air during sample processing.

Table 3
Sizes of ZnS**1** and ZnS**2** nanoparticles estimated from TEM analysis.

ZnS nanoparticles	Sheet		Cylinder	
	Width (nm)	Length (nm)	Diameter (nm)	Length (nm)
ZnS**1**	69–155	122–273	90–108	137–232
ZnS**2**	127–200	127–339	39–138	214–465

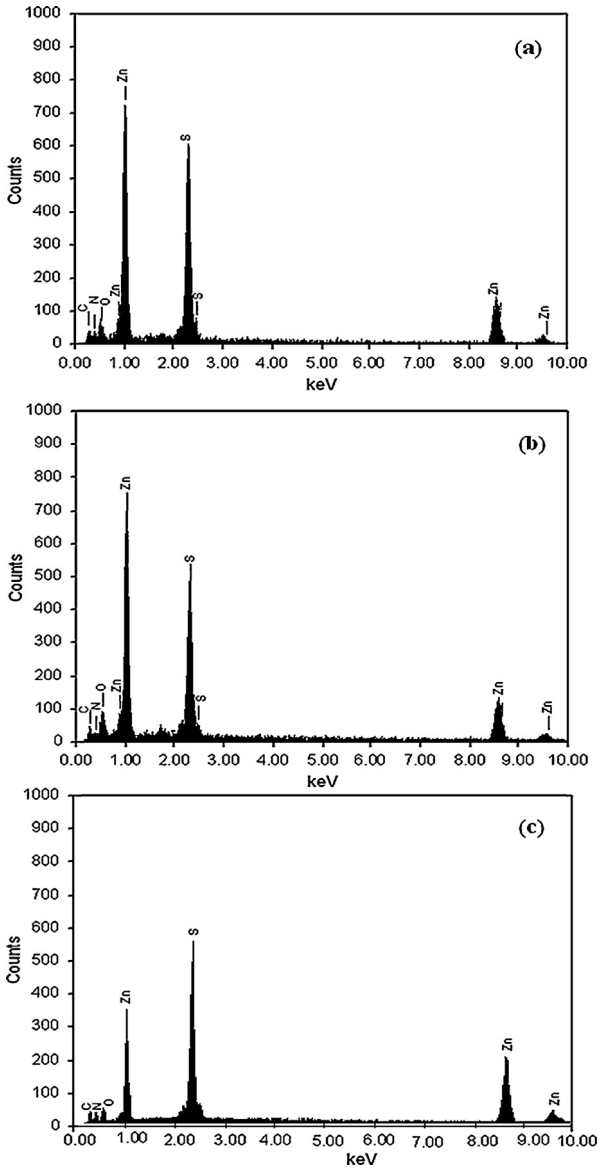

Fig. 3. EDAX spectra of (a) ZnS**1**, (b) ZnS**2**, and (c) ZnS**3**.

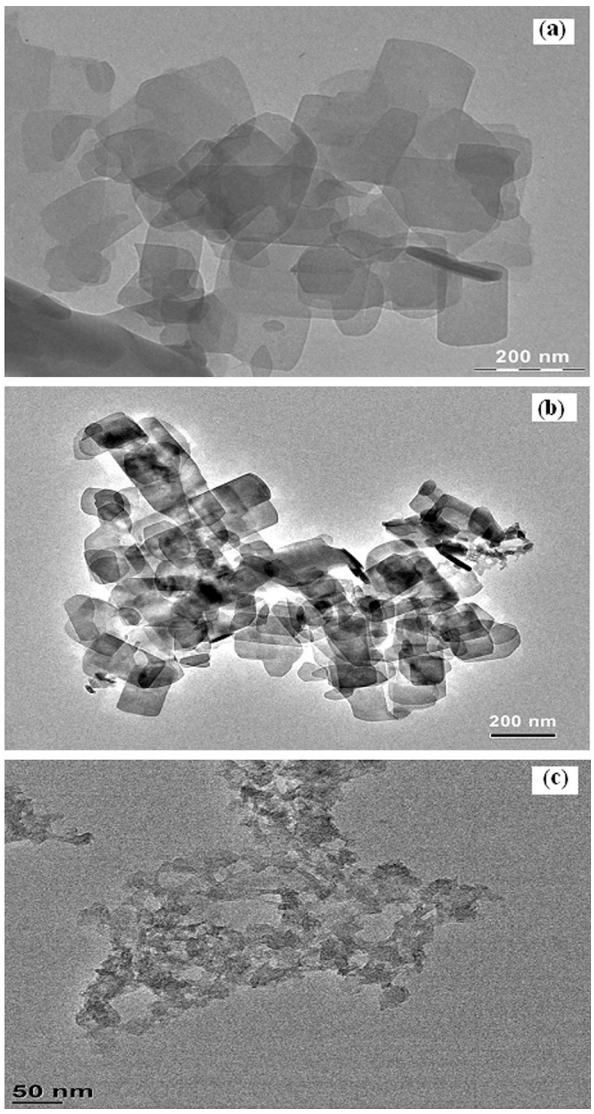

Fig. 4. TEM images of (a) ZnS**1**, (b) ZnS**2**, and (c) ZnS**3**.

3.1.3. Transmission electron microscopy (TEM) studies

The dimensions and morphologies of the zinc sulfides were studied by TEM measurements. TEM images of ZnS**1**, ZnS**2** and ZnS**3** are shown in Fig. 4. The results of the TEM studies are summarized in Table 3. The TEM images show that two types of morphologies are present in ZnS**1** and ZnS**2**. The TEM images of ZnS**1** and ZnS**2** show that the particles are sheet- and cylinder-like structures. The TEM image of the ZnS**3** sample shows that the nanoparticles are partly interconnected, whereas each individual particle possesses an irregular shape. The length of the sheets and cylinders in ZnS**2** are longer than those in ZnS**1**. This may be due to the presence of pyridine in the precursor ($Zn(thqdtc)_2(py)$). The morphology of ZnS**3** is different from those of ZnS**1** and ZnS**2**. This indicates that the dithiocarbamate ligands in metal complex (precursor) affect the shape and size of the nanoparticles.

3.1.4. Optical properties

To investigate the optical properties of the obtained ZnS nanoparticles, the room temperature UV–vis absorption and fluorescence spectra were recorded. The UV–visible absorption spectra of ZnS nanoparticles prepared from different precursors are shown in Fig. 5. Absorption maxima were observed at 250 (4.96 eV), 240 (5.17 eV), and 245 nm (5.06 eV) for ZnS**1**, ZnS**2** and ZnS**3**, respectively. The absorption peaks are significantly blue-shifted relative to bulk ZnS (344 nm) [24], indicating quantum confinement.

The fluorescence spectra of the ZnS nanoparticles are shown in Fig. 6. The fluorescence spectra of ZnS**1**, ZnS**2** and ZnS**3** nanoparticles exhibit only one broad emission peak through the excitation at 350 nm. The broad emission peak

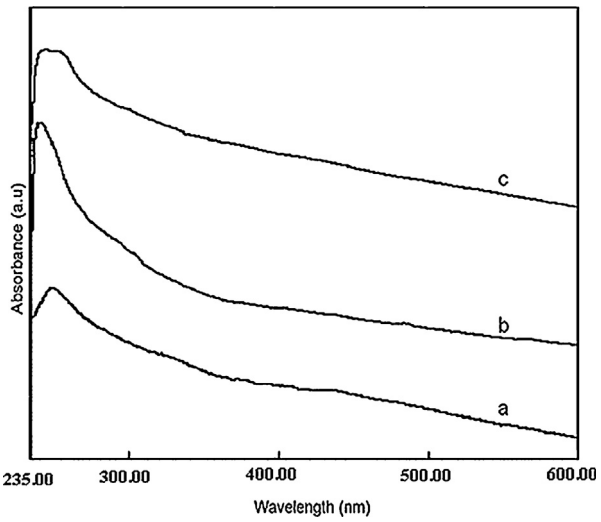

Fig. 5. Absorption spectra of (a) ZnS**1**, (b) ZnS**2**, and (c) ZnS**3**.

around 440 nm was assigned to the electron–hole recombination from internal vacancies for Zn and S atoms. It is observed that there is a prominent blue shift of around 35 nm of the emission band compared with that of the bulk ZnS [25], which might be due to the quantum size effects of the ZnS nanocrystals.

3.2. Structural analysis of precursor Zn(thqdtc)$_2$

The ORTEP diagram of Zn(thqdtc)$_2$ is shown in Fig. 7. The Zn(thqdtc)$_2$ complex is monomeric with two molecules per unit cell. The molecular structure of Zn(thqdtc)$_2$ features two chelating dithiocarbamate ligands with Zn–S distances relatively narrow at 2.3024(9) to 2.3530(12) Å. The distorted tetrahedral

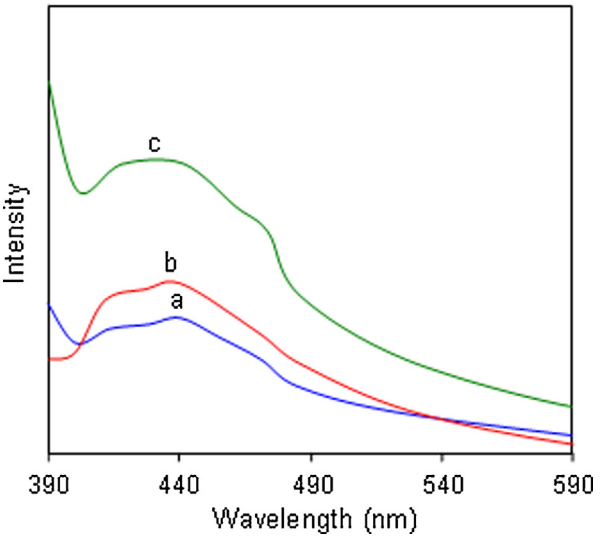

Fig. 6. Fluorescence spectra of (λ_{ex} = 350 nm): (a) ZnS**1**, (b) ZnS**2**, and (c) ZnS**3**.

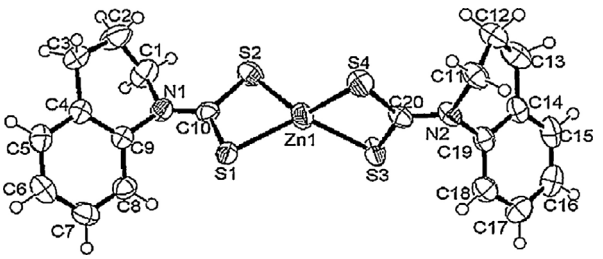

Fig. 7. ORTEP diagram of precursor [Zn(thqdtc)$_2$].

coordination geometry is evidenced around the zinc atom as attested to by the S–Zn–S angles of 77.87(2) to 128.84(3)°. This complex represents an example of a monomeric structure of the zinc dithiocarbamates, which are usually dimeric [26]. The short thioureide C–N distance, 1.327(3) Å, indicates that the π electron density is delocalized over the S_2CN moiety and that the bond has a significant double-bond character. The C–S distances [1.721(2) Å] are to a considerable extent shorter than the typical C–S single-bond distance 1.81 Å. Therefore, all the C–S bonds in the present structure possess the partial double bond character observed in most of the dithiocarbamates. The C–C and C–N bond distances associated with the tetrahydroquinoline moiety are normal. Thus, the overall solid-state structure is similar to that of the other known examples of monomeric binary zinc dithiocarbamates, viz., Zn(S_2CN(Me)Cy)$_2$ [27] and Zn($S_2CN(CH_2Ph)_2$)$_2$ [28].

4. Conclusions

We reported here a simple and versatile method for the controlled synthesis of zinc sulfide nanoparticles using three new single source precursors in a single-pot and low-temperature process. Only triethylenetetramine (trien) has been used as a capping agent. The sheet and cylinder shape of ZnS nanoparticles were obtained from Zn(thqdtc)$_2$ and Zn(thqdtc)$_2$(py), whereas shapeless nanoparticles were obtained with Zn(thiqdtc)$_2$(py). It is clear from these reactions that the ligands in the metal complexes affect the shape and size of the nanoparticles. This method may be extended to the fabrication of nanoparticles with various shapes and sizes exhibiting novel morphologies and properties using metal complexes containing various dithiocarbamate ligands as precursors.

References

[1] X. Peng, L. Manna, W. Yang, J. Wickham, E. Schere, A. Kadacanich, A.P. Alivisatos, Nature 404 (2000) 59.
[2] J.T. Hu, T.W. Odom, C.M. Lieber, Acc. Chem. Res. 32 (1999) 435.
[3] F. Kim, S. Kwan, J. Akana, P.D. Yang, J. Am. Chem. Soc. 123 (2001) 4360.
[4] J.T. Hu, L.S. Li, W.D. Yang, L. Manna, A.P. Alivisatos, Science 292 (2001) 2060.
[5] N. Tessler, V. Medvedev, M. Kazes, S. Kan, U. Banin, Science 295 (2002) 1506.
[6] W.C.W. Chan, S. Nie, Science 281 (1998) 2016.
[7] V.F. Puntes, K.M. Krishnan, A.P. Alivisatos, Science 291 (2001) 2115.
[8] T. Hyeon, S.S. Lee, J. Park, Y. Chung, N. Bin, J. Am. Chem. Soc. 123 (2001) 12798.

[9] Y.N. Xia, P.D. Yang, Y.G. Sun, Y.Y. Wu, B. Mayers, B. Gates, et al. Adv. Mater. 15 (2003) 353.
[10] J.L. Yuan, K. Kajiyoshi, K. Yanagisawa, H. Sasaoka, K. Nishimura, Mater. Lett. 60 (2006) 1284.
[11] T. Kuzuya, Y. Tai, S. Yamamuro, K. Sumiyama, Sci. Technol. Adv. Mater. 6 (2005) 84.
[12] J. Li, Y. Xu, D. Wu, Y. Sun, Solid State Commun. 130 (2004) 619.
[13] M.H. Ullah, C.S. Ha, J. Nanosci. Nanotechnol. 5 (2005) 1376.
[14] K.Y. Gao, H. Karl, I. Grosshans, W. Hipp, B. Stritzker, Nucl. Instrum. Methods Phys. Res. B 196 (2002) 68.
[15] M. Behboudnia, A. Habibi-Yangjeh, Y. Jafari-Tarzanag, A. Khodayari, J. Cryst. Growth 310 (2008) 4544.
[16] N.V. Hullavarad, S.S. Hullavarad, P.C. Karulkar, J. Nanosci. Nanotechnol. 8 (2008) 3272.
[17] D. Fan, M. Afzad, M.A. Malik, C.Q. Nguyen, P. O'Brien, P.J. Thomas, Coord. Chem. Rev. 251 (2007) 1878.
[18] N. Srinivasan, S. Thirumaran, Superlattices Microstruct. 51 (2012) 912.
[19] A.A. Memon, M. Afzaal, M.A. Malik, C.Q. Nguyen, P. O'Brien, J. Raffery, Dalton Trans. (2006) 4499.
[20] A. Altomare, M.C. Burla, M. Camalli, G. Cascavano, G. Giacovazzo, A. Guagliardi, G. Polidori, J. Appl. Crystallogr. 27 (1994) 4385.
[21] G.M. Sheldrick, SHELXL-97, University of Göttingen, Göttingen, Germany, 1997.
[22] B.S. Garg, R.K. Garg, M.J. Reddy, Indian J. Chem. A 32 (1993) 697.
[23] N. Srinivasan, S. Thirumaran, S. Ciattini, J. Mol. Struct. 921 (2009) 63.
[24] P.E. Lippers, M. Lanhoo, Phys. Rev. B 39 (1989) 10935.
[25] P. Yang, M.K. Lu, F.Q. Meng, C.F. Song, D. Xu, Opt. Mater. 27 (2004) 103.
[26] G. Hogarth, Prog. Inorg. Chem. 53 (2005) 73.
[27] M. Yin Chan, C.S. Lai, E.R.T. Tiekink, Appl. Organomet. Chem. 18 (2004) 298.
[28] A. Decken, R.A. Gossage, M. Yin Chan, C.S. Lai, E.R.T. Tiekink, Appl. Organomet. Chem. 18 (2004) 101.